Effects of topography and crustal heterogeneities on the source estimation of LP event at Kilauea volcano

Simone Cesca, Jean Battaglia, T. Dahm, E. Tessmer, S. Heimann, P. Okubo

Geophys. J. Int. (2008) **172,** 1219–1236 doi: 10.1111/j.1365-246X.2007.03695.x

Effects of topography and crustal heterogeneities on the source estimation of LP event at Kilauea volcano

S. Cesca,[1,3] J. Battaglia,[2] T. Dahm,[3] E. Tessmer,[3] S. Heimann[3] and P. Okubo[4]

[1] *Seismological Central Observatory Gräfenberg Erlangen, BGR, Germany. E-mail: simone.cesca@zmaw.de*
[2] *Laboratoire Magmas et Volcans, Université Blaise Pascal, CNRS, Clernont-Ferrand, France*
[3] *Institut für Geophysik, University of Hamburg, Hamburg, Germany*
[4] *U.S. Geological Survey, Hawaiian Volcano Observatory, Hawaii National Park, Hawaii, USA*

Accepted 2007 November 22. Received 2007 November 14; in original form 2007 June 19

SUMMARY

The main goal of this study is to improve the modelling of the source mechanism associated with the generation of long period (LP) signals in volcanic areas. Our intent is to evaluate the effects that detailed structural features of the volcanic models play in the generation of LP signal and the consequent retrieval of LP source characteristics. In particular, effects associated with the presence of topography and crustal heterogeneities are here studied in detail. We focus our study on a LP event observed at Kilauea volcano, Hawaii, in 2001 May. A detailed analysis of this event and its source modelling is accompanied by a set of synthetic tests, which aim to evaluate the effects of topography and the presence of low velocity shallow layers in the source region. The forward problem of Green's function generation is solved numerically following a pseudo-spectral approach, assuming different 3-D models. The inversion is done in the frequency domain and the resulting source mechanism is represented by the sum of two time-dependent terms: a full moment tensor and a single force. Synthetic tests show how characteristic velocity structures, associated with shallow sources, may be partially responsible for the generation of the observed long-lasting ringing waveforms. When applying the inversion technique to Kilauea LP data set, inversions carried out for different crustal models led to very similar source geometries, indicating a subhorizontal cracks. On the other hand, the source time function and its duration are significantly different for different models. These results support the indication of a strong influence of crustal layering on the generation of the LP signal, while the assumption of homogeneous velocity model may bring to misleading results.

Key words. Earthquake source observations; Volcano seismology; Wave propagation.

1 INTRODUCTION

The occurrence of so-called long period (LP) events in volcanic areas is a current topic of research and the definition of source models and the interpretation of physical phenomena to explain their features is still a matter of debate. Moreover, since different models associate their occurrence with fluid movement beneath volcanoes, they may play an important role as precursors of eruptions and volcanic activity. The general term 'LP event' is actually used to describe a wide set of seismic signals, with the common characteristic of a nearly monochromatic frequency content, in the range between 0.5 and 5 Hz (Chouet 1996). Different models have been proposed to describe the physical process that could be responsible for their generation; these models are typically associated with the resonance of fluid-filled cavities and cracks, with different geometries.

The interpretation of LP seismograms by the inversion of broadband seismic data requires taking into account effects of seismic wave propagation in volcanic areas. This task requires the use of numerical methods to estimate the effects of complex features, which play a major role in these areas. Typically, due to the short epicentral distances of available stations, both near- and far-field terms have to be calculated. Additionally, effects of topography and local heterogeneities of the crustal structure have to be considered. As the majority of the proposed models include effects of topography, but make the assumption of homogeneous velocity models, the retrieved source characteristics could be affected by these simplifications.

In this study, we compare the effects of different crustal models, considering both the forward problem of the generation of synthetic seismograms as well as the inversion problem of source retrieval. The study is applied to a LP signal observed at Kilauea Caldera in 2001 May. Our final goal is to evaluate the effects of crustal structures on the observed ringing seismograms, in order to improve the source inversion for LP events and distinguish between source and path effects in the generation of LP signals.

2 LP EVENT AT KILAUEA: DATA ANALYSIS

As a case study, we will focus on the source of a LP signal recorded below the summit of Kilauea volcano. This volcano has been erupting for more than 20 years. The eruption which began on 1983 January 3 takes place on the east rift zone at the Pu'u O'o eruption crater, about 15 km from the summit. The seismic activity below the summit includes permanent tremor and occasional LP events. This activity is assumed to be related to the transit of magma below the summit toward the rift zone and the eruption site. In recent years, on several occasions, small volcanic crisis occurred below the summit, characterized by deformations and an increase of seismic activity. These events are assumed to be caused by surges in the magma flux (Cervelli & Miklius 2003). The seismic source of shallow LP events and the associated signals at Kilauea volcano have been widely studied using different techniques (e.g. Saccorotti *et al.* 2001; Almendros *et al.* 2001a,b, 2002). All these studies agree on the epicentral location of the seismic source, common for tremor and LP signals, which is identified at the northeastern border of Halemaumau crater. Saccorotti *et al.* (2001) estimated a very shallow source depth (∼100 m) for the LP events, while a deeper origin of tremor. Almendros *et al.* (2001b) analysed a wide set of data issued from seismic arrays installed at Kilauea Caldera in 1997 February, locating different source clusters. The major one, including more than 75 per cent of the considered events, is located 200 m northeast of Halemaumau, with a shallow depth at less than 200 m below the caldera floor. Finally, Almendros *et al*. (2002) identified different components, which contribute to the wave fields recorded at Kilauea volcano, the dominant being body waves generated at shallow depth and epicentral location consistent with previous studies. Surface waves generated along the path to the seismic antennas also contribute to the observed wave field. Owing to the location, depth and size of the source region and the known existence of a hydrothermal system permeating the volcanic edifice and the caldera (Ingebritsen & Scholl 1993), Almendros *et al*. (2001b, 2002) concluded that the observed LP seismicity has a hydrothermal origin. In particular, Almendros *et al.* (2001b) suggested that the LP seismicity could reflect the response of the hydrothermal system to magma transport in a deeper conduit.

The LP event we focus on was recorded on 2001 May 21, at about 2:57 UT. Some examples of observed displacements are shown in Fig. 1. The signal was recorded as a sporadic event during a short volcanic crisis which lasted for about 90 min between 2:25 and 3:55 UT. The crisis was characterized by an increase of the tremor and long period activity, accompanied by the rapid inflation of a shallow source below the summit (Cervelli & Miklius 2003). This short crisis was part of a longer duration 'tilt event' as it was preceded by a period of slow inflation, which lasted about 15 hr, and was followed by a deflation lasting for about 20 hr, which brought the tilt level to almost the initial pre-event value. This pulse of activity was accompanied with a short delay by comparable deformations and a surge in the effusion rate at Pu'u O'o eruption crater. While the relation of the LP event to the seismic crisis cannot be judged at this point of the study, the spectral characteristics and large amplitude of the event make it outstanding in the crisis.

A preliminary source location was obtained using a location technique based on the use of seismic amplitudes corrected for site effects (Battaglia & Aki 2003). This method, which was previously applied to the location of shallow and intermediate LP events (Battaglia *et al.* 2003), uses the decay of the amplitude of body waves

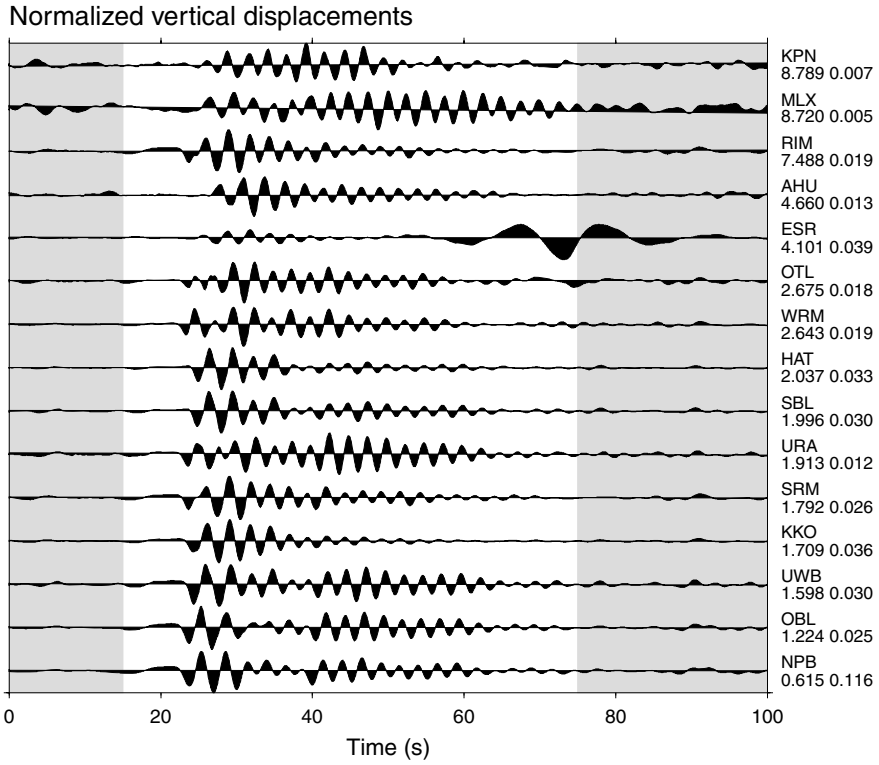

Figure 1. Displacement seismograms for the studied LP event at several seismic stations. Vertical components are shown as normalized traces with station name, epicentral distance (in km) and maximal amplitude (in mm) indicated on the right side of each trace. The time intervals used for source inversions are highlighted with a white background.

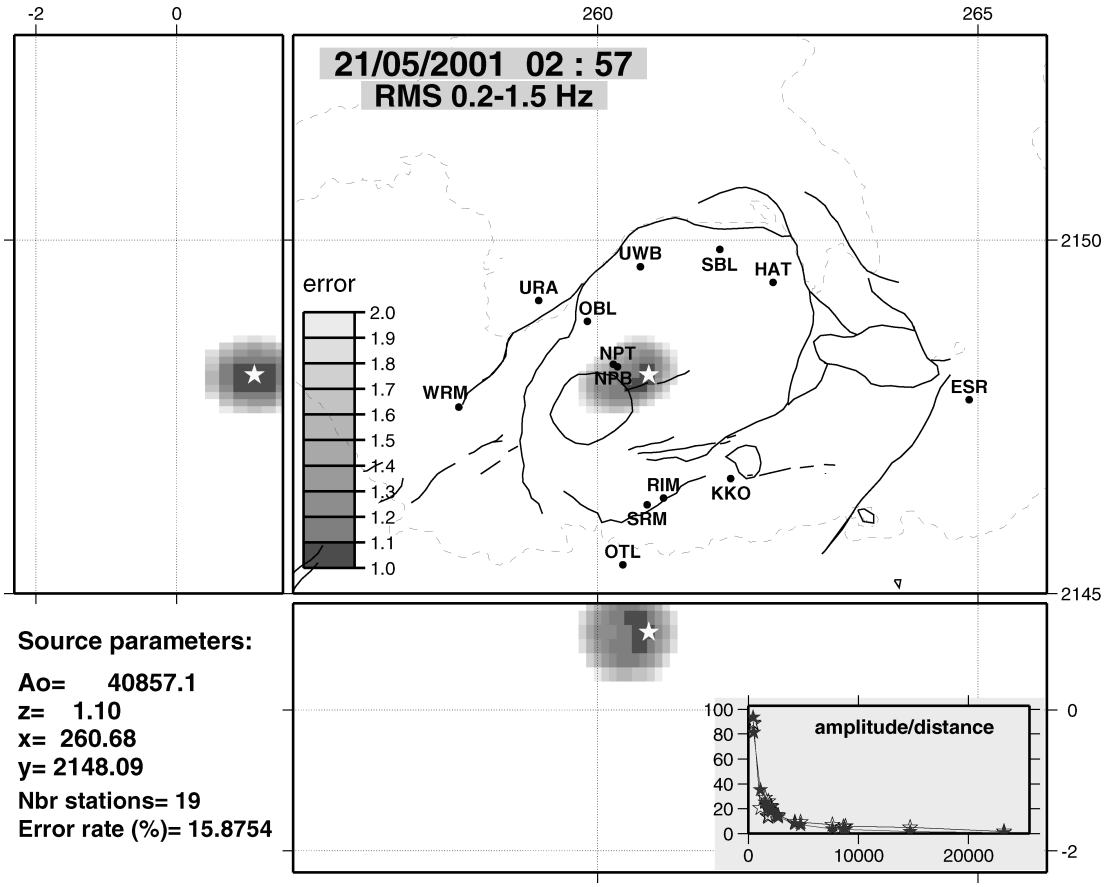

Figure 2. Source location for the LP event, obtained by inverting the spatial distribution of seismic amplitudes calculated peak to peak. Source location (white star) and its error (grey scale) are plotted both for the horizontal projection and for the north–south and the east–west vertical cross sections. The figure shows the station locations (black dots), as well as the Caldera border and the main geological features. The retrieved source parameters are indicated in the bottom left-hand corner and the fit of the seismic amplitude versus epicentral distance is given in the bottom right corner: empty starts represent the observations and black stars represent the calculated amplitudes.

as a function of hypocentral distance to infer the source location. In this case we use signals recorded by 19 stations, including short period and broadband stations. We calculate amplitudes peak-to-peak on the whole unfiltered LP traces after correcting for the instrument responses of the different sensors and acquisition chains. We find a source located at 2148.0 km north and 260.8 km east (UTM coordinates), close to the northeastern rim of Halemaumau crater (Fig. 2). The use of amplitudes calculated using rms formula on the whole unfiltered waveforms instead of peak to peak amplitudes lead to comparable results. The location program indicates a source at very shallow depth, 10 m below the caldera surface. We note that this depth may, however, be underestimated, possibly because of the use of a simplified amplitude decay, which does not take into account the near-field decay. On the other hand, the epicentral location is consistent with those estimated by Ohminato *et al.* (1998), Saccorotti *et al.* (2001), Almendros *et al.* (2001b), Battaglia *et al.* (2003) and Kumagai *et al.* (2005), studying similarly shallow events at Kilauea caldera. We also note, that the epicentral location is in good agreement with the location of the deformation source at the origin of the inflation observed during the seismic crisis (Cervelli & Miklius 2003), but it is found shallower in comparison to their source estimated at 855 m a.s.l.

The LP signal was recorded at 27 seismic stations, including broadband and short period stations, all located on the Big Island, Hawaii. The signal was visible as far as at 35–40 km from the epicentre, at stations DAN, MOK and SWR, which are located on the flank and close to the summit of Mauna Loa volcano. Owing to the problems arising by dealing with crustal model of large spatial extension, and also observing that the number of stations with a good signal-to-noise ratio decreases significantly with the epicentral distance, a compromise was taken by reducing the study area to a 15×15 km^2 delimited by the UTM coordinates 253–268 km east and 2139–2154 km north (Fig. 3). The choice of this region allows the inclusion of a maximum number of stations for the selected area size. A larger square of 25×25 km with the same centre is used for numerical simulations as we need to add an external region for defining the absorbing boundaries of the model. However, synthetic seismograms will not be calculated in the external region, its topography will be taken into account and its effects considered only in the inner area. The main topographic features of this region are related to the NW–SE slope of the Mauna Loa volcano flank, and the presence of the Kilauea caldera. Finally, after removal of saturated traces, data from 17 stations (Fig. 3) located in the inner area could be used, providing 36 traces. The combined use of data issued from both short period and broadband stations is considered reasonable after comparing the seismic signals at stations NPB and NPT, which are closely located and have different instrumentation. The comparison of velocity traces after correcting for instrument responses shows almost identical waveforms with a cross-correlation coefficient for the vertical components equal to 0.95. This gives

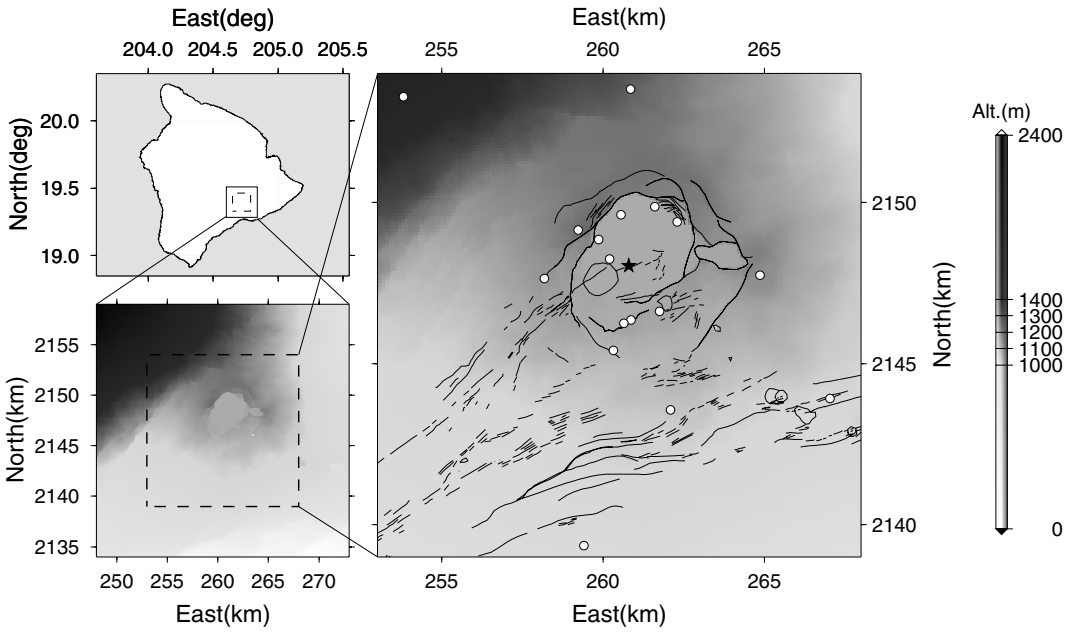

Figure 3. Area of study. Top left-hand panel: map of the Big Island of Hawaii showing the area of the study: the continuous line represents the 25 × 25 km area including the absorbing boundary, while the dashed line corresponds to the inner 15 × 15 km area. Bottom left-hand panel: enlarged plot of the area under study, topography is represented in tones of grey (the scale is plotted on the right side of the figure). Right-hand panel: enlarged plot of the inner area, showing the topography (tones of grey), the major fractures and geological features, including Kilauea caldera border and the inner Halemaumau crater (black lines), as well as station locations (white circles) and the epicentral location of LP event (black star).

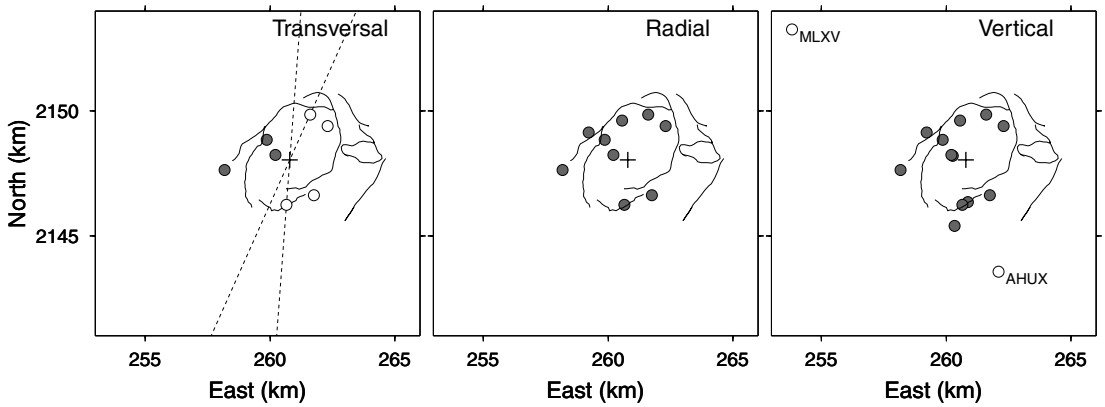

Figure 4. Results of first motion polarity analysis. The three plots correspond, respectively, from left to right, to polarities for transversal, radial and vertical components. In each plot positive (grey circles) and negative (white circles) polarities are shown for each station and the epicentral location of the LP event is indicated as a black cross. The range of azimuthal directions (dashed lines) separating positive and negative polarities is also shown for the transversal component.

indications for a source located closer to NPT station, where the signal is observed 0.2 s before than that at station NPB.

The spectral analysis shows common features for LP waveforms recorded at all stations and components: signals are nearly monochromatic, with a dominant frequency of 0.40–0.45 Hz, and most of the radiated energy is related to the frequency range between 0.1 and 0.7 Hz. These features distinguish the LP event under study from those analysed by Almendros *et al.* (2002b, 2002), which contained energies in the band 1–15 Hz, with dominant peaks between 2 and 6 Hz. Looking for possible indications of characteristic radiation patterns, the information supplied by the amplitude of the seismic signals was analysed. After rotating the velocity traces to the radial and transversal axes, the signs of the first large pulse were plotted (Fig. 4). We note that the polarities which we plot may not correspond to the first arrival pulses because most signals are emergent with small amplitude first pulses hidden in the background tremor. Instead, we use the polarity of the first high amplitude pulse, which is commonly observed at most stations. Some interesting considerations arise from this analysis. First, we can mention that the observed amplitudes of radial and vertical components (although not plotted in Fig. 4) decrease with the epicentral distance, giving a rough support to the estimated epicentral location. A strong amplitude reduction through the caldera rim, which would give indication of a significant velocity contrast, cannot be clearly deduced and evaluated by these data. More information arises from the analysis of the polarities. A change in polarities, between stations located inside and outside of the caldera, suggests wave conversion at horizontal layers or lateral discontinuities at the caldera rim. On the other hand,

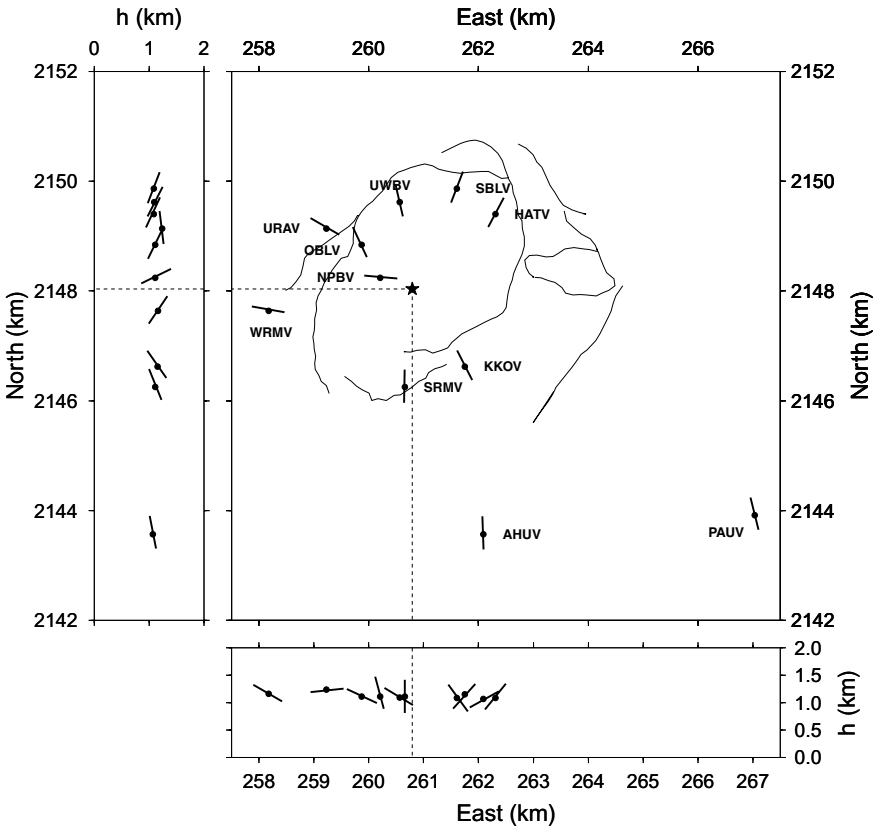

Figure 5. Particle motion analysis. The direction of particle motion during 7.5 s time windows starting at the LP signal is represented at the location of each station as a thick continuous line. The particle motions are plotted both for the horizontal projection and for the north–south and east–west cross sections.

a different behaviour of transversal components, with respect to a N–NE striking direction seems to be related to a radiation pattern of the source.

An analysis of particle motion was finally made to examine the polarization of signal onsets at each station. This may give additional indications with respect to the source location, and is therefore, a useful test to check the predicted location on the basis of a different approach. Results of this analysis, which was carried out using data windows of 7.5 s including the first part of the signal, are summarized in Fig. 5. The figure shows the directions of the linear polarization of the signals at each station, with respect to the horizontal plane, north–south and east–west vertical sections. Directions of linear polarization were corrected for the effects of the free surface (Neuberg & Pointer 2000). The validity of the previously retrieved epicentral location is confirmed by these results. Additionally, by backtracing the ray paths under the assumption of a layered model, the source depth, which was relatively poorly constrained by the previously discussed location technique, could be estimated. The average of the retrieved depths, obtained by using the polarization of each signal, point to a source depth of 130 m below the free surface, corresponding to about 980 m altitude above the sea level. For this process, a flat layered crustal model for Kilauea caldera was used, based on the results of Saccorotti *et al.* (2003); this model is presented and discussed below.

3 INVERSION METHOD

The method to retrieve source components of a time dependent seismic source in a volcanic area is based on the inversion of the following equation, which gives the displacement field $\underline{u}$ at a position $\underline{x}$ and at time t from an internal composite seismic point source acting at position $\underline{\xi}$ and at time τ:

$$u_n(\underline{x}, t) = M_{pq}(\underline{\xi}, \tau) * G_{np,q}(\underline{x}, t; \underline{\xi}, \tau) + F_p(\underline{\xi}, \tau) * G_{np}(\underline{x}, t; \underline{\xi}, \tau). \quad (1)$$

In the above equation, M_{pq} are moment tensor components, F_p single force components and G_{np} are Green's functions; summation convention is applied and delimitations between indexes represent spatial partial derivatives. Eq. (1) basically expresses the displacement field as the time convolution of source mechanism terms (F_p and M_{pq}) with terms taking into account the wave propagation in the modelled media (G_{np} or their spatial derivatives). It has to be remembered that eq. (1) differs from the classical representation of the displacement due to a seismic point source (e.g. as in Aki & Richards 1980), since the source here includes a single force term. This source term has to be added to describe properly a more general seismic source for a volcanic event, as external forces have to be added to the conservation of moment in the source volume. Such forces may indeed be involved in the source process when fluids are quickly removed from the source at depth, or when material is blown off the volcano during an eruption. The complete solution of the forward problem, according to eq. (1), corresponds to the calculation of 27 Green's functions (GF) for each station used: 18 for the moment tensor (MT) and 9 for the single forces (SF). These GFs correspond to three components of the ground motion in response to 9 basic point sources (6 MT components and 3 SF components), thus are sufficient to reconstruct synthetic seismograms for any combination of basic sources.

The inverse problem can be solved in the frequency domain by inverting several small-size matrices, one for each sampled frequency ω_i (Auger *et al.* 2006, Cesca & Dahm 2008):

$$u_n(\omega_i) = m_p(\omega_i)\, g_{np}(\omega_i). \quad (2)$$

Note that in the short formulation of eq. (2), m is a vector of length 9 and represents either MT or SF, while g represents either GFs or their spatial derivatives. The time dependency of each retrieved source component is in principle independent. It can be expected that the components of the MT, which correspond to the same physical phenomena (e.g. slip on a fault, explosion, etc.), should have the same time history. Similarly, SF components should have the same time-dependency. These two constraints are handled by our inversion algorithm, by means of a singular value decomposition of the source matrix (Vasco 1989; Cesca & Dahm 2008). As a result, MT and SF solutions will be expressed under the following constraints:

$$\begin{aligned} M_{pq}(t) &= M^*_{pq} f_m(t) \\ F_p(t) &= F^*_p f_f(t), \end{aligned} \quad (3)$$

where $f_m(t)$ and $f_f(t)$ express the time dependency of MT and SF components, respectively, while M^* and F^* define signs and amplitudes of different source components. Errors in the retrieved solutions may be estimated following a bootstrap approach, testing the response of several (in this case 200) perturbed solutions; a detailed description of the method can be found in Cesca & Dahm (2008).

In the following cases, we will apply the described approach. In a first inversion, unconstrained source components will be retrieved, based on solutions of eq. (2). Synthetic seismograms will be calculated for this solution, which we can refer to as the 'unconstrained' solution. Misfit is estimated by comparing observed and synthetic seismograms using a L^2 norm. This way, the inversion technique is more weighted on the fit of traces with larger amplitudes. We think this is an advantage, especially in a volcanic area, as traces with lower amplitudes either pertain to far stations, for which model anomalies over longer source–receiver paths can not be well reproduced, or show a poorer signal-to-noise ratio. However, on the base of the recommendation of Ohminato *et al.* (1998) and Chouet *et al.* (2003), to check the reliability of our best inversion results, we will present additional results using an alternative fitting procedure, which gives to the time traces a distance-dependent weight, linearly increasing with the epicentral distance. Although slightly different to the methodology proposed by Ohminato *et al.* (1998) and Chouet *et al.* (2003), our technique is based on a similar approach.

In a second step, the unconstrained solution is decomposed using singular value decomposition, under the constraint expressed by eq. (3), obtaining a so-called 'constrained' solution. The comparison of constrained and unconstrained solutions may add important information toward a better understanding of the source mechanism and the physical phenomena driving the generation of LP signals. While an unconstrained source will always lead to a better fit of the data, it may require a complex description of the source mechanism, for which each source component have a different dependence on time. More likely, the source behaviour can be well approximated by a constrained source, in which components share a common time evolution. A good indicator of the reliability of the constrained solution to describe the source mechanism is given by the fit between constrained and unconstrained source components. When the constrained solution fits the unconstrained one, the source process can be more simply explained by means of two physical phenomena, one described by a moment tensor and the other by a single force. In this case, the focal mechanism can be interpreted on the base of the coefficients M^*_{pq} and F^*_p (eq. 3), which respectively, describe the moment tensor configuration and single force orientation, while the time evolutions of the two sources (moment tensor and single force) are, respectively, described by the functions $f_m(t)$ and $f_f(t)$, defined in eq. (3).

4 EFFECTS OF LAYERED MODELS

A major goal of this study is to evaluate the effects of crustal heterogeneities on the inversion of the seismic source for LP events. Most published results on the source mechanism of such events describe the crustal model by means of a homogeneous velocity structure, eventually considering topographic effects, and relate the observed long-lasting ringing signal to a periodic ringing of the source. Since the classical equation for the displacement at the surface (eq. 1) relates the seismograms to the source mechanism and to the wave propagation, the observed ringing may depend on both these terms. The choice of a homogeneous model, and the consequent simplification of the wave propagation behaviour in such a medium, may lead to the conclusion that the ringing has necessarily to depend on the time behaviour of the focal mechanism. This result is often valid, considering that small-scale heterogeneities do not affect the wave propagation when wavelengths are sufficiently larger than heterogeneities sizes. On the other hand, in our case, the source depth is very shallow, and the shallow crustal structure at the epicentral region is known to be composed of low velocity layers associated with the poorly consolidated volcanic products. In such a medium, it can be expected that excited signals will be characterized by shorter wavelengths, which will be affected by a heterogeneous structure. Forward modelling of synthetic seismograms has been extensively discussed by Goldstein & Chouet (1994), in order to explain volcanic tremor at Pu'u O'o crater, Kilauea volcano. The authors showed how, in presence of shallow sources (with a depth lower than 100 m), the resonance in the near-surface layers, possibly combined with resonating sources, may well explain the observations. Effects of layered structure on the synthetic seismogram may be so strong as to hide differences related to different source mechanisms. The effects of low-velocity shallow layers have also been studied for the case of basins by Hill & Levander (1984), Olsen *et al.* (1995) and Wen *et al.* (2007), among others. These studies showed that a major effect of the presence of shallow sources in soft sediments and low-velocity layers is the generation of significant surface waves and ringing phases, and a significant increase of the duration of signals. Similar effects have been shown for the case of interface (Scholte) waves propagating at the seafloor in presence of low-velocity mushy layers (e.g. Nguyen *et al.* 2007). The effects of these heterogeneities in the velocity structure may be even more important than those related to the topography. Effects of different topographic features on seismic waveforms have been discussed by several authors (e.g. Geli *et al.* 1988; Bouchon *et al.* 1996; Ashford *et al.* 1997; Wen *et al.* 2007) and specific applications to volcanic areas have highlighted major effects in presence of a steep topography (e.g. Ohminato & Chouet 1997; Neuberg & Pointer 2000; Ripperger *et al.* 2003; Cesca *et al.* 2007).

Before deriving the source mechanism by the inversion of seismic signals for complex 3-D models, it is important to quantify the possible effects of heterogeneous structures on the characteristics of the expected seismograms. To achieve this goal, we proceeded with some synthetic tests considering various simplified 2-D structural velocity models with the preliminary assumption of a flat surface. The choice of such simplified models allows us to examine the

effects of the different crustal structures on the excitation of ringing phases. This way, these effects can be distinguished from those related to topography, which is introduced subsequently. The first considered model, referred as KHOM, is an homogeneous model used for volcanic source inversion at Kilauea (Ohminato *et al.* 1998). The knowledge of the shallow crustal structure at Kilauea is mostly gained from the caldera area (e.g. Dawson *et al.* 1999; Saccorotti *et al.* 2003), while tomographic studies for a wider area (Monteiller *et al.* 2005) do not provide detailed information for the uppermost crustal structure. As a consequence, a simplified layered model may be derived only for the caldera area, on the base of the work of Saccorotti *et al.* (2003). For the external area, we consider two possible cases, assuming either a simple homogeneous model or maintaining the layering derived for the caldera. In this way, two models are proposed: model KLAY is a flat layered model (basically a 1-D model) composed of three layers with a total thickness of 410 m over a half-space, while model KCAL uses the same layering for a 3 km width caldera and is homogeneous outside. The layered structure which we use has been obtained by averaging two models proposed by Saccorotti *et al.* (2003) for two areas of the caldera region. Because of computational costs, our numerical modelling does not allow considering layers with small thickness. Therefore, the two uppermost layers of Saccorotti *et al.* (2003) have been here simplified in a unique layer of 60 m thickness, with an averaged *S*-wave velocity of 550 m s^{-1}. *P*-wave velocity structure has been originally defined in order to keep a constant ratio with *S*-wave velocity in agreement with Ohminato *et al.* (1998). In the layers where this value would be lower than *P*-wave velocity in water, this has been fixed to a common value of 1800 m s^{-1}. The seismic source is assumed to be a purely isotropic implosive source, with a Gaussian-shaped source time function (STF) of 0.5 s. Although isotropic sources do not excite primary *S* waves, the *S*-wave structure will control the propagation of converted *S* and Rayleigh waves. Note that the definition used here for the STF duration refers to its half length, meaning that the excited radiation is mainly below 1Hz. Results are presented assuming four possible seismic source depths: 40, 100, 300 and 600 m. The choice of source depths arises from the intention of this study to focus on the case of very shallow sources. On the other hand, they have been chosen according to the crustal models, in order to have the source embedded in all the defined layers and in the lower half-space. Source magnitudes are the same for all models, but are not described here in detail, since we are interested in a qualitative analysis of waveforms generated by different sources and models and only show normalized time traces. Synthetic seismograms of 10 s duration have been then obtained by applying a numerical algorithm based on the pseudo-spectral method (Tessmer *et al.* 1992; Heimann 2005). Radial and vertical components of synthetic seismograms have been calculated for a line of recorders crossing the caldera border, and therefore, allow the direct comparison of the effects of this border on wave propagation for different velocity models.

The three chosen models and the resulting synthetic seismograms are shown in Fig. 6 (source depth 40 m, vertical and radial components) and Fig. 7 (source depths of 40, 100, 300 and 600 m, only vertical component). From both figures it can be easily seen how the introduction of layered structures, both for models KLAY and KCAL, affects the synthetic waveforms. Synthetic seismograms for model KHOM present a very simple behaviour, only characterized by a *P* phase for closer stations and *P* and *sP* phases at more distant stations. In contrast, the presence of shallow low velocity layers in model KLAY and KCAL is responsible for the generation of significant surface waves. This result shows how a shallow source located in such models can then reproduce a ringing seismogram, even assuming a simple time behaviour of the source (here, a smooth pulse and an isotropic source). A comparison of synthetic seismograms for KLAY and KCAL models, show how the first model is characterized by a larger dispersion of the surface waves, depending on the epicentral distance. Model KCAL, on the contrary, predicts a minor dispersion, when crossing the caldera border. Another characteristic effect of this model is the generation of additional delayed energetic pulses, which are related to the interference of waveform reflected at the caldera rim. The comparison of synthetic seismograms for different source depths shows how surface waves are generated, when assuming layered models, independently on the source depths, as all selected sources considered here are very shallow. A variation in the frequency content is observed for the shallowest source: in this case the seismic source, embedded in a low velocity layer, is responsible for the generation of higher frequency signals. As an extreme case, we have run a last simulation assuming a layered model with a very low *S*-wave velocity in the uppermost layer; we have used values derived by Nguyen *et al.* (2007) for unconsolidated sediment at the seafloor ($Vs = 200$ m s^{-1}, $Vp = 1600$ m s^{-1}). Results indicate that the extremely low shear wave velocity and the velocity contrast at the interface below the source (60 m depth) significantly increase the duration of the ringing waveform. For example, assuming a fully layered model, the ringing on the vertical component lasts about 10 s, for the new model, versus a duration lower than 2 s, for KLAY model (Fig. 6). Similar conclusions follow the comparison of layered models accounting for the caldera size.

Due to the characteristic frequency content of the studied signal, which has a nearly monochromatic behaviour, it is of interest to analyse how different model parameters may control the synthetic spectra. Above, we have discussed the combined effect of the source depth and the velocity structure on the synthetic waveforms. Two other parameters, which can play an important role in this respect, are the size of the caldera, if assuming the KCAL model, and the length of the STF. Two sets of tests are discussed below assuming the KCAL model and a source depth of 100 m. As mentioned previously, an important effect introduced by the Caldera model is the signal associated with the interference of reflected waveforms travelling backwards from the rim. As Kilauea Caldera has an almost elliptical shape, the wave propagation behaviour could be different depending on the considered direction. To check the effects of a change in the caldera width, we have compared simulations assuming model KCAL and two modified models, which have a lateral extension of the layered area of 2 and 4 km, respectively. Results are shown in Fig. 8. Synthetic seismograms for the considered models are unchanged in the first 2–3 s, slight variations can be observed in the last part of the waveform. These differences depend on the variable interference of waves reflected at the caldera border, due to the variation of the caldera size (when leaving the other model parameters unchanged). The observed differences do not have a large impact, as also indicated by the analysis of the amplitude spectra, which are almost unchanged by varying the caldera width. This behaviour is observed both at station 2, which is located in the layered area, and at station 6, which is located outside.

Similarly, we have carried out a comparison of the synthetic waveforms and their frequency content, by changing the duration of the excitation signal. Three tests have been made, assuming source time functions of 0.5, 1.0 and 2.0 s, while the other parameters of the models were kept unchanged (model KCAL, source depth $h = 100$ m). Results are shown in Fig. 9. It is straightforward to observe how the shortest STF generates a higher frequency radiation. Owing to the smaller wavelengths of the seismic radiation, the wave propagation

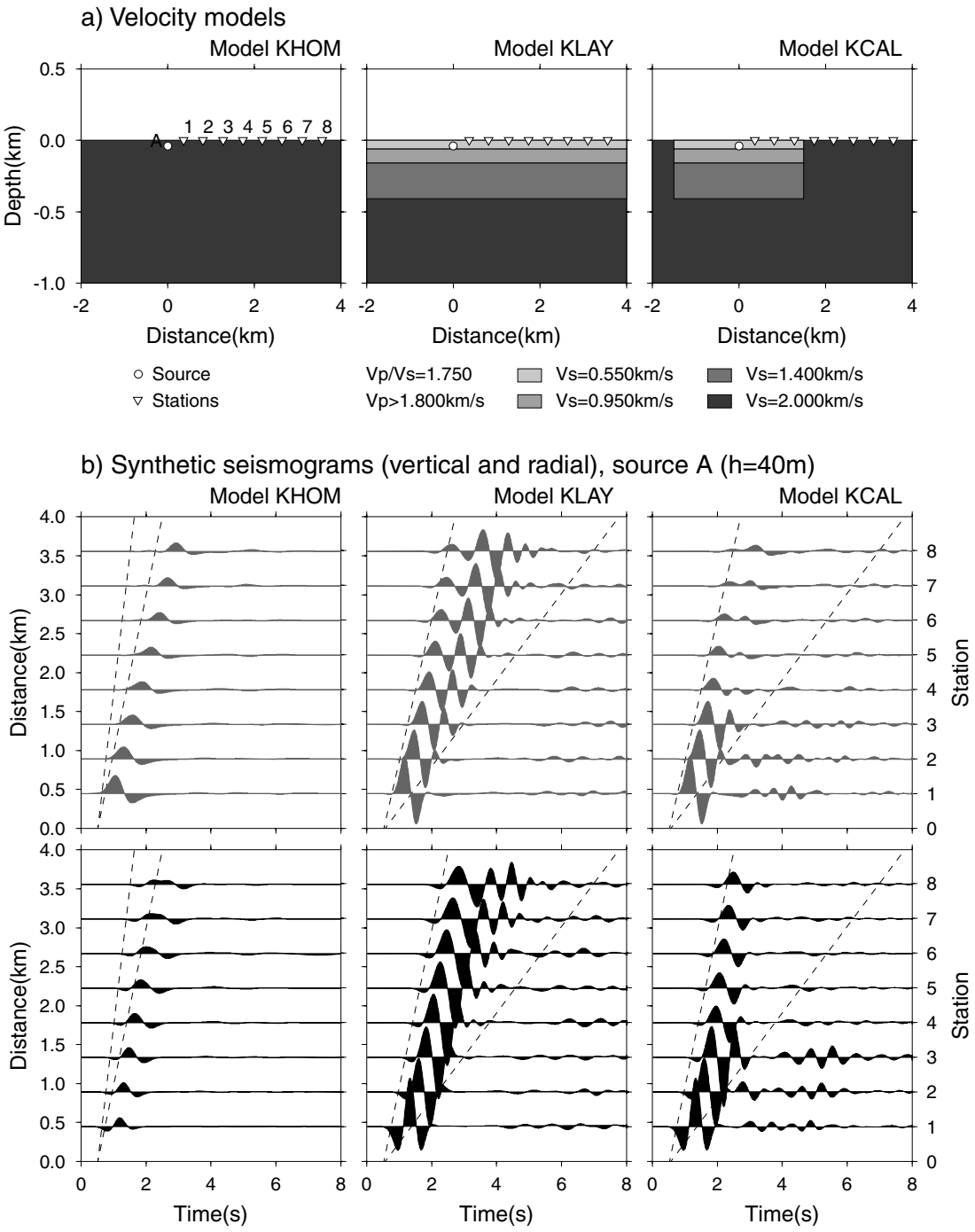

Figure 6. Forward modelling for different crustal models. (a) Velocity models KHOM (left-hand panel), KLAY (centre panel) and KCAL (right-hand panel) showing *S*-wave velocities and the station (triangles named 1–8)/source (circle named A) layout. (b) Synthetic seismograms obtained for an implosive source at location A ($h = 40$ m) for the three models (from left-to-right-hand panel) and for the vertical (grey) and the radial (black) components. The eight traces in each plot correspond to the different stations whose name is given on the left vertical axis. Theoretical arrival times for direct *P* and *S* waves are also plotted thin dashed lines. Amplitudes of seismograms are all normalized to the same value.

is strongly affected by the velocity structure, resulting in ringing seismograms, both in the radial and the vertical components, and especially for the closest stations. In contrast, effects of the caldera layering and the velocity discontinuity are negligible in the case of the longer STF. The observed characteristics of the synthetic waveforms are reflected in their amplitude spectra: independently on the spatial components (vertical and radial), the progressive reduction of the STF length results in the inclusion of higher frequencies in the signal, and the shift of the dominant and cut-off frequency to larger values.

Effects of crustal layering have been studied carefully by a set of synthetic tests, showing how the combined effects of shallow sources and shallow low velocity structures could explain, at least partially, the observed ringing phases. These results indicate that the

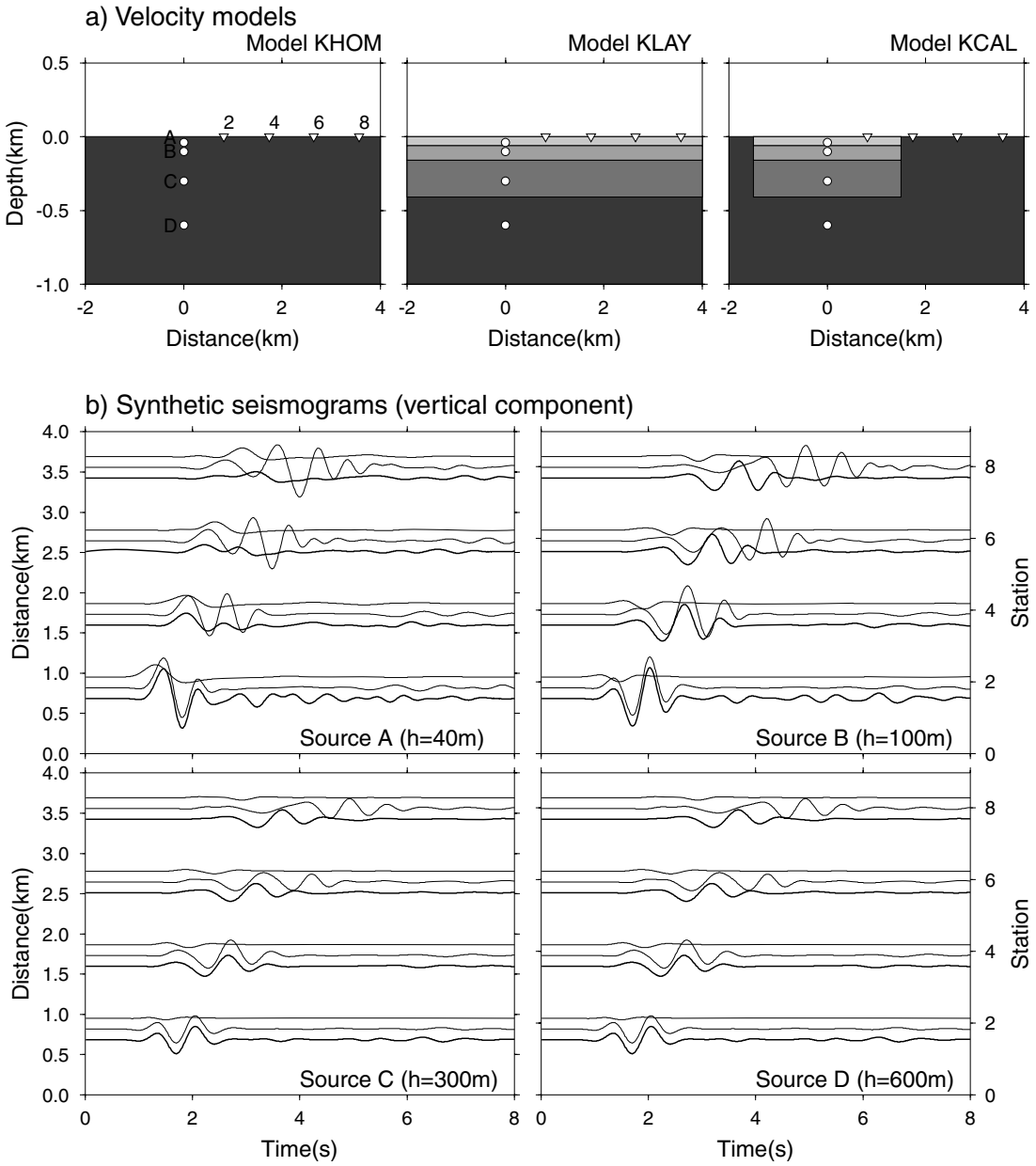

Figure 7. Forward modelling for different source depths. (a) Velocity models KHOM (left-hand panel), KLAY (centre panel) and KCAL (right-hand panel) showing *S*-wave velocities as tones of grey (scale in Fig. 6), station locations (triangles numbered 2–8) and source locations (circles with letters A–D). (b) Vertical components of synthetic seismograms obtained for an implosive source at position A (top left-hand panel), B (top right-hand panel), C (bottom left-hand panel) and D (bottom right-hand panel). Four sets of traces are plotted for each source location, relative to the four stations whose name is indicated on the left vertical axis. Each set of traces represents synthetic seismograms for model KHOM (top trace, thin line), KLAY (central trace, medium line) and KCAL (bottom trace, thick line). Amplitudes of seismograms are all normalized to the same value (the same as in Fig. 6).

retrieved source in any inversion problem dealing with LP signals could strongly depend on the assumptions on the crustal structure. Our results suggest that a careful choice of the crustal model, or at least a comparison of results for different models is preferable before deriving definitive conclusions on a source model, which could lead to erroneous interpretations. We have shown that the frequency content of predicted seismograms is mostly affected by the source depth, the velocity structure and the time length of the excitation pulse. In contrast, if assuming a layered model for the caldera embedded in a homogeneous half-space, it resulted that the size of the caldera plays a minor role.

5 SOURCE INVERSION

5.1 Inversion for 1-D models

As a preliminary step, before including the effects of topography in a 3-D modelling, we make a set of source inversion for simplified flat 1-D models. The goal of these inversions is to have a first check of the possible effects of layered models on the time behaviour of the retrieved source. In previous section it has been shown how for a shallow source in a layered crustal model the synthetic seismograms can partially reproduce the observed ringing of the LP signal. However, it has still to be verified if the difference

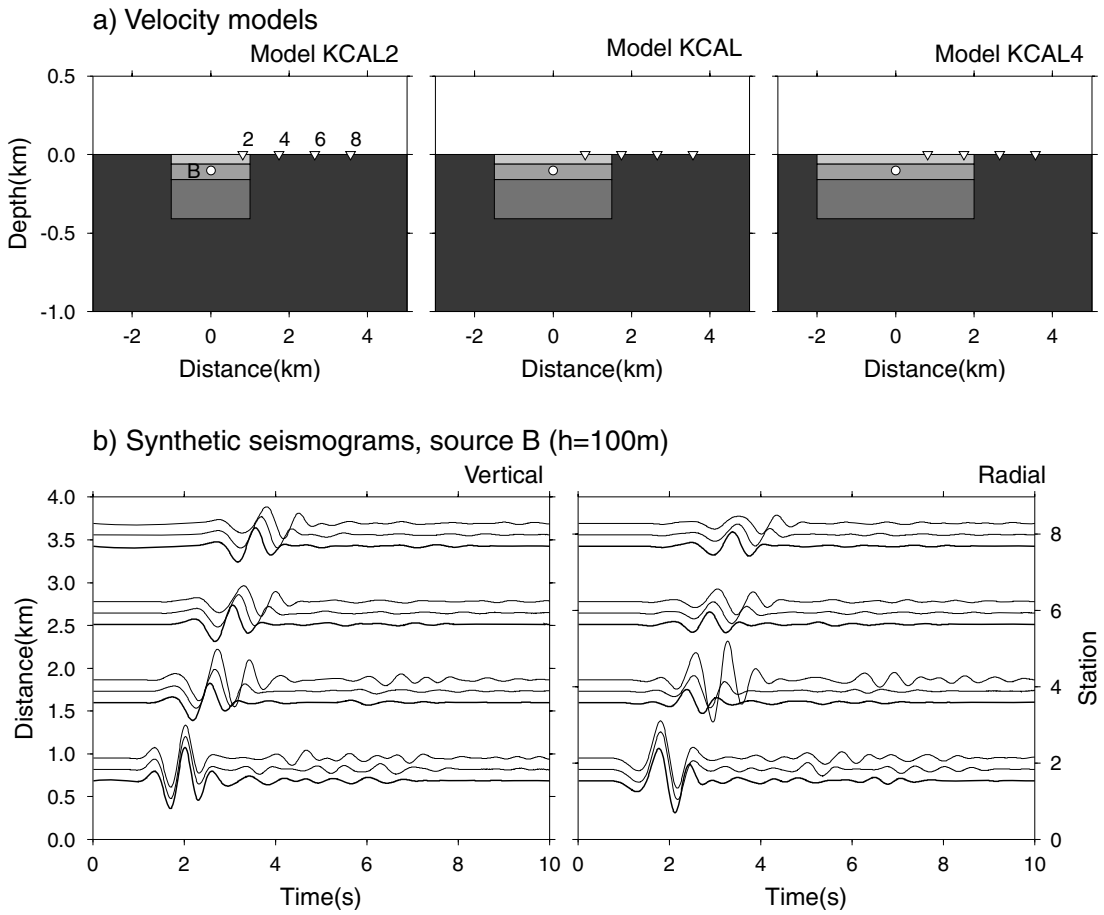

Figure 8. Forward modelling: effects of caldera size. (a) Velocity models KCAL2 (left-hand panel), KCAL (centre panel) and KCAL4 (right-hand panel) showing *S*-wave velocities as tones of grey (scale in Fig. 6), station locations (triangles numbered 2–8) and source location (circle B). (b) Vertical (left-hand panel) and radial (right-hand panel) components of synthetic seismograms obtained for an implosive source at position B ($h = 100$ m). Four sets of traces are plotted, relative to the four stations (named on the left vertical axis). Each set of traces represents synthetic seismograms for model KCAL2 (top trace, thin line), KCAL (central trace, medium line) and KCAL4 (bottom trace, thick line). Amplitudes of seismograms are all normalized to the same value (the same as in Fig. 6).

in the GFs obtained for homogeneous and layered media, may result in significant differences in the inverted sources. A second goal of the presented inversion tests with 1-D models is to better constrain the source depth. Since the computational time requirements to do a 3-D modelling makes at the moment unrealistic the comparison of different models with different source depths (although, this can be in future improved by using reciprocity theorem and calculating station-to-source GFs), the comparison is done for simplified 1-D models, which can be handled in a convenient time. An advantage of assuming simplified 1-D models is the possibility to evaluate the effects of structural heterogeneities and layering, distinguishing them to those related to topography. Basically, for each model, different sets of GFs are obtained for a set of possible depths, the source is then inverted for each depth and the analysis of results give indications both on the source behaviour and the depth for which the best fit of the data is found. These tests add significant information and constraint on the source depth, which is particularly important for the following 3-D modelling.

The calculation of GFs for flat models is a reasonable approach for a preliminary estimation of the inverted source location when only stations close to the epicentre are considered. In the area of the caldera the topography is relatively smooth, and effects of topography should be small. We only consider eight stations, which are located in the caldera, with an epicentral distance below 2.5 km. Station locations have a good azimuthal coverage (maximum azimuthal gap 107°) and a similar altitude ($\Delta h < 80$ m). A reflectivity method (Müller 1985) was used to calculate GFs. Since only horizontally layered media can be implemented in this approach, we only use models KHOM and KLAY, as defined previously. The reflectivity code allows a fast estimation of full waveform GFs, including near- and far-field terms, and is therefore, especially suitable to compare inversion results under the assumption of different source depths. A set of inversions was made, following the methodology explained in paragraph 3, assuming the two models and source depths up to 1 km. Source depth is varied by 25 m, up to 100 m depth, and by 100 m steps, below this. When assuming a homogeneous model (KHOM) the best fit, equal to 0.466, is obtained for a source located at 300 m depth. On the other hand, when considering model KLAY, we obtain the best fit (0.337) for a depth of 50 m. A summary of the two resulting best sources is shown in Fig. 10 by plotting the source time functions for moment tensor and single force components (constraints, eq. 3). In both cases, the excited source is dominated by the three dipoles and the vertical force components, while double couple and horizontal force components are negligible. Horizontal dipoles show similar behaviour, having larger amplitudes than the vertical dipole; the relative amplitudes between horizontal and vertical dipoles are

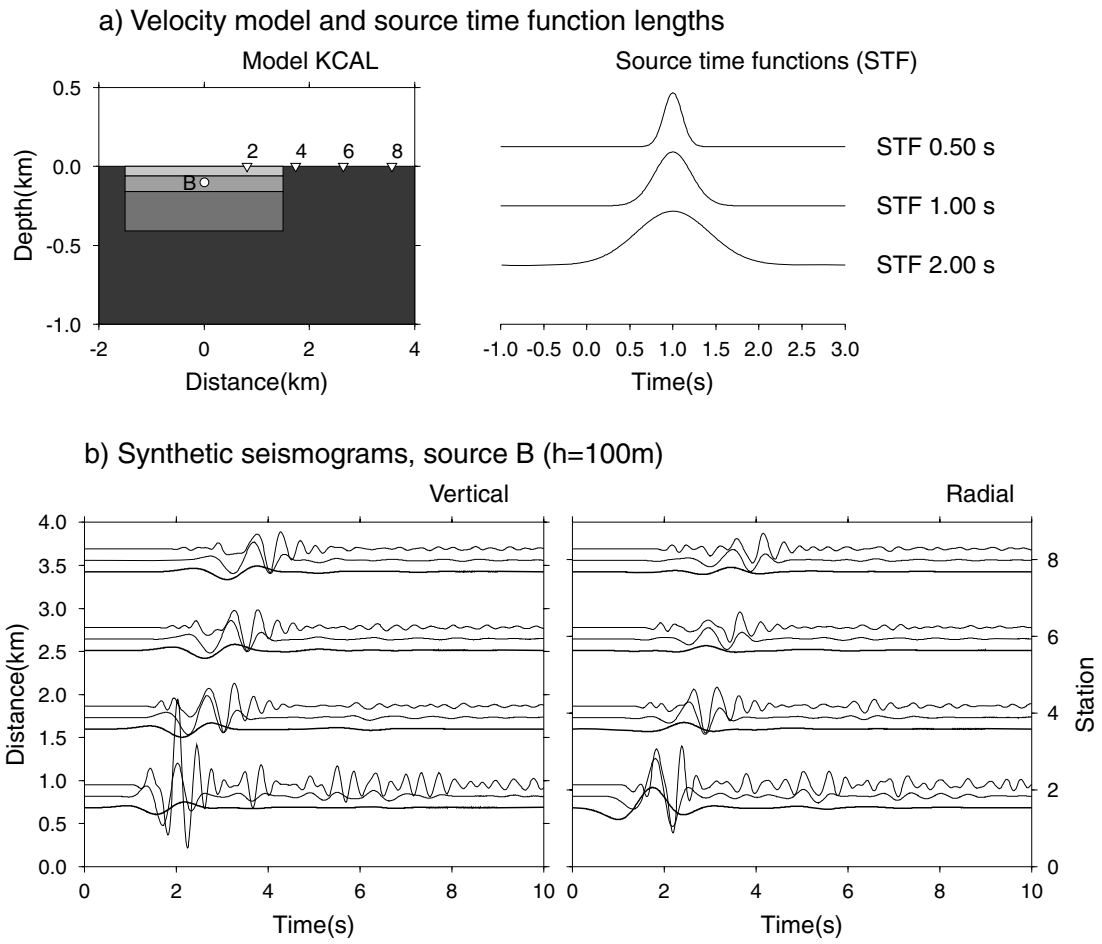

Figure 9. Forward modelling: effects of the duration of the excitation signal. (a) Left-hand panel: velocity model KCAL showing *S*-wave velocities as tomes of grey (scale in Fig. 6), station locations (triangles numbered 2–8) and source location (circle B). Right-hand panel: shape and duration of the three considered source time functions. (b) Vertical (left-hand panel) and radial (right-hand panel) components of synthetic seismograms obtained for an implosive source at position B ($h = 100$ m). Four sets of traces are plotted, relative to the four stations (named on the left vertical axis). Each set of traces represents synthetic seismograms for source time functions of 0.50 s (top trace, thin line), 1.00 s (central trace, medium line) and 2.00 s (bottom trace, thick line). Amplitudes of seismograms are all normalized to the same value (the same as in Fig. 6).

in the order of 1.5 and 2 for model KLAY and KHOM, respectively. In Fig. 10, the eigenvectors for the retrieved solution, scaled with their eigenvalues are also plotted; note that they do not vary in time, as a consequence of the constraint on source time functions. From the comparison of the results, we observe how both models predict a source associated with the vibration of a cavity, whose geometry appears to be almost vertically symmetric with an additional vertical force. The relative amplitude between horizontal and vertical components is not fitting the expected behaviour of a horizontal crack source, for which the contribution of the vertical dipole component should be dominant. While the focal mechanism is very similar for both crustal models, its time behaviour is quite different. The ringing of the source lasts much longer, for about 45 s, in the case of model KHOM, while the release of energy at the source decreases much faster, mostly in the first 10 s, in the solution obtained for model KLAY. This result indicates how the complexity of the observed seismograms is mostly associated with the source behaviour when assuming a simplified homogeneous crustal model, while it depends both on source and propagation effects, when introducing a more realistic layering.

We repeated the inversion process for model KLAY, using an alternative fitting procedure, to increase the weighting of distant stations and obtained similar results. The geometry of the focal mechanism remains stable, while the time behaviour of the source time function lasts slightly longer. The majority of the energy is still radiated in the first 10–20 s, considerably faster than what observed using a homogeneous model. Finally, we observe in both cases of model KHOM and KLAY, that the source time functions of the moment tensor and single force components have a similar behaviour. The cross-correlation coefficients between STFs are equal to 0.87 and 0.76 for model KHOM and KLAY, respectively. These results may indicate that both sources (moment and force) are associated with the same physical phenomenon, or to different phenomena with a similar time evolution. More likely, these results support a different interpretation: the inversion approach could be unable to distinguish between force and moment effects, at least for the chosen geometry of crustal model and station locations. This second possibility would indicate that the obtained vertical force is artificially retrieved, owing to the fact that its radiation pattern is very similar to the one produced by a vertical dipole for stations located above the hypocentre, at very short distances. This interpretation would explain the retrieval of an underestimated vertical dipole, with respect to the one predicted for a crack, as part of it would be erroneously associated with a vertical force. A last consideration, supporting the presented hypothesis,

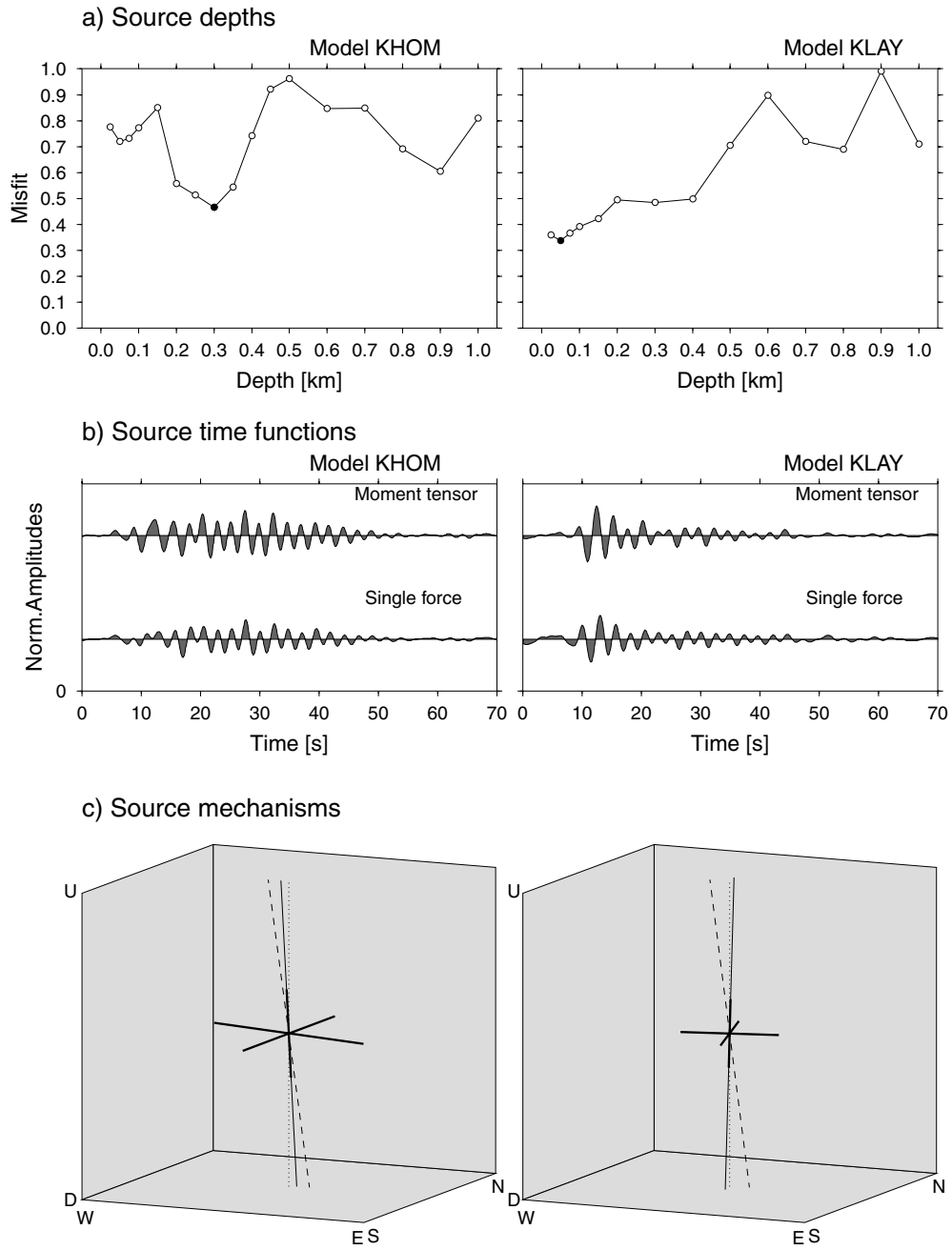

Figure 10. Solutions of 1-D inversion. (a) Misfit versus source depths (thin line and white circles) when assuming flat models KHOM (left-hand panel) and KLAY (right-hand panel); best solutions are identified by black circles. (b) Normalized source time functions (STFs) retrieved when assuming model KHOM (left-hand panel) and KLAY (right-hand panel) for moment tensor and single force components (respectively, top and bottom). (c) Orientation of eigenvectors (thick continuous lines), when assuming model KHOM (left-hand panel) and KLAY (right-hand panel). Amplitudes of eigenvectors are scaled to respective eigenvalues and crack axis (thin continuous line), force direction (dashed line) and vertical direction (dotted line) are also shown.

concerns the difficulty of giving a physical interpretation to a vertical force associated with a horizontal crack: in such a geometry, an eventual fluid movement associated with a force component would be more likely expected in a direction parallel to the crack plane. The Akaike Information Criterion (Akaike 1974) supports our interpretation, at least for the solution obtained with the homogeneous model, indicating that the improvement of the fit achieved assuming a more complex source (moment tensor and single force) is not significant towards the increase of the number of free parameters, which are needed to describe it.

5.2 Inversion for 3-D models

The last step of the source study for the LP event is the most complete and requires the generation of GFs for 3-D crustal models, taking into account effects of topography as well as possible velocity structures. To determine theoretical GFs we use a numerical method based on pseudo-spectral approach (Tessmer *et al.* 1992). The domain has an extension of 25 × 25 km (Fig. 11), composed of an inner 15 × 15 km area of study and 5 km width absorbing boundaries. The previously described crustal models are considered,

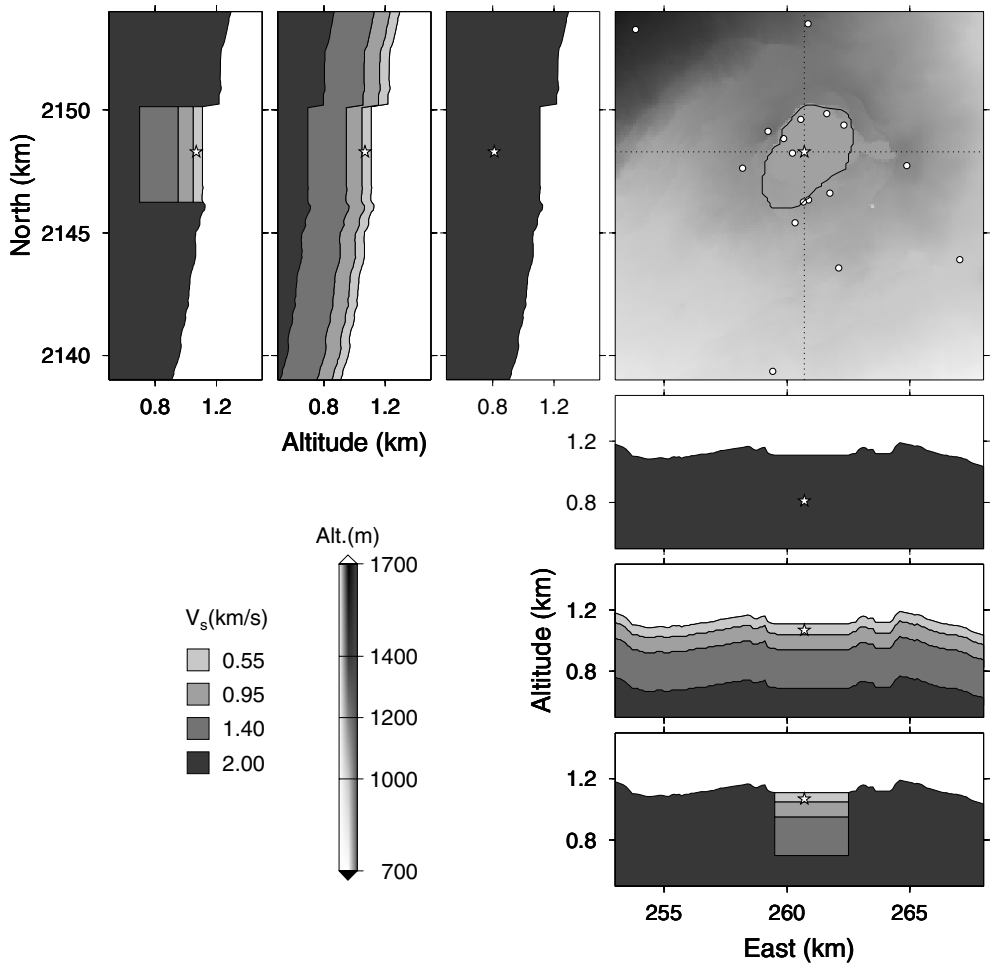

Figure 11. 3-D velocity models. Inner area (15 × 15 km) and cross sections for the three possible crustal models (KCAL, KLAY and KHOM, respectively from left to right, in the NS cross sections, and from bottom to top, in the EW cross-sections). The LP source location is represented with a star. The topography is plotted on the map view and the *S*-wave velocity structure are plotted on the cross-sections. Both plots use grey tones, but they refer to two different scales, shown on the bottom right corner of the figure.

although now they include topography. Cross-sections of the used models, which will be referred again as KHOM, KLAY and KCAL, are also plotted in Fig. 11. An almost-elliptical horizontal extension of the Caldera is assumed for model KCAL, according to the realistic extension of Kilauea Caldera. GFs are calculated with a sampling rate of 10 ms, assuming the three possible models and for the source depths, the values retrieved in the previous paragraph ($h = 300$ m for model KHOM, $h = 50$ m for both layered models KLAY and KCAL).

Inversions have been carried out using 36 data windows of 70 s duration, starting about 5 s before the onset of the LP event. Data and GFs are both filtered during the inversion, between 0.1 and 0.6 Hz. A summary of the inversion results, with the plot of the complete set of fitted seismograms for the three inversions, is shown in Fig. 12. Although the number of traces is large, synthetic seismograms can well reproduce the observed LP data, both for vertical and horizontal components. A better fit is observed for larger amplitude seismograms (e.g. at stations NPB, SBL, UWB and NPT), as a consequence of the larger weight attributed to those signals in the inversion. On the other hand, for some of the more distant stations (e.g. at AHU), the time evolution of the signal is not fitted, possibly due to time shifts introduced by local structures or lateral discontinuity, which cannot be reproduced. Misfit results are equal to 0.544, 0.592 and 0.792, for models KHOM, KCAL and KLAY, respectively. While the first two models present a better fit, the worse fit obtained for the layered model KLAY may indicate that the chosen model is not properly describing the real velocity structure outside the caldera. Misfit values reflect the difficulty of reproducing observations for a very large number of data (36 time traces), and could be improved by reducing the number of inverted traces. Nevertheless, we considered that the use of all available data is important to better constrain the inverted source mechanism. The comparison of synthetics and observations for the best fitting models (Fig. 12) is satisfactory, especially at the nearest stations and for those traces with larger amplitudes.

The source mechanism for each inversion can be identified on the basis of the constrained solution (eq. 3), assuming a common behaviour for moment tensor components, which we will refer as moment tensor source time function (STF), and a different one for single forces. The singular value decomposition allows the description of the source behaviour by means of a moment tensor, a single force, and their two STFs. To ensure the validity of this approach, we checked the fit between the constrained and the unconstrained solutions for each of the three cases and always obtained values lower than 0.1 (using L^2 norm). The comparison of STFs (Fig. 13, top) clearly confirms the behaviour suggested by the synthetic tests,

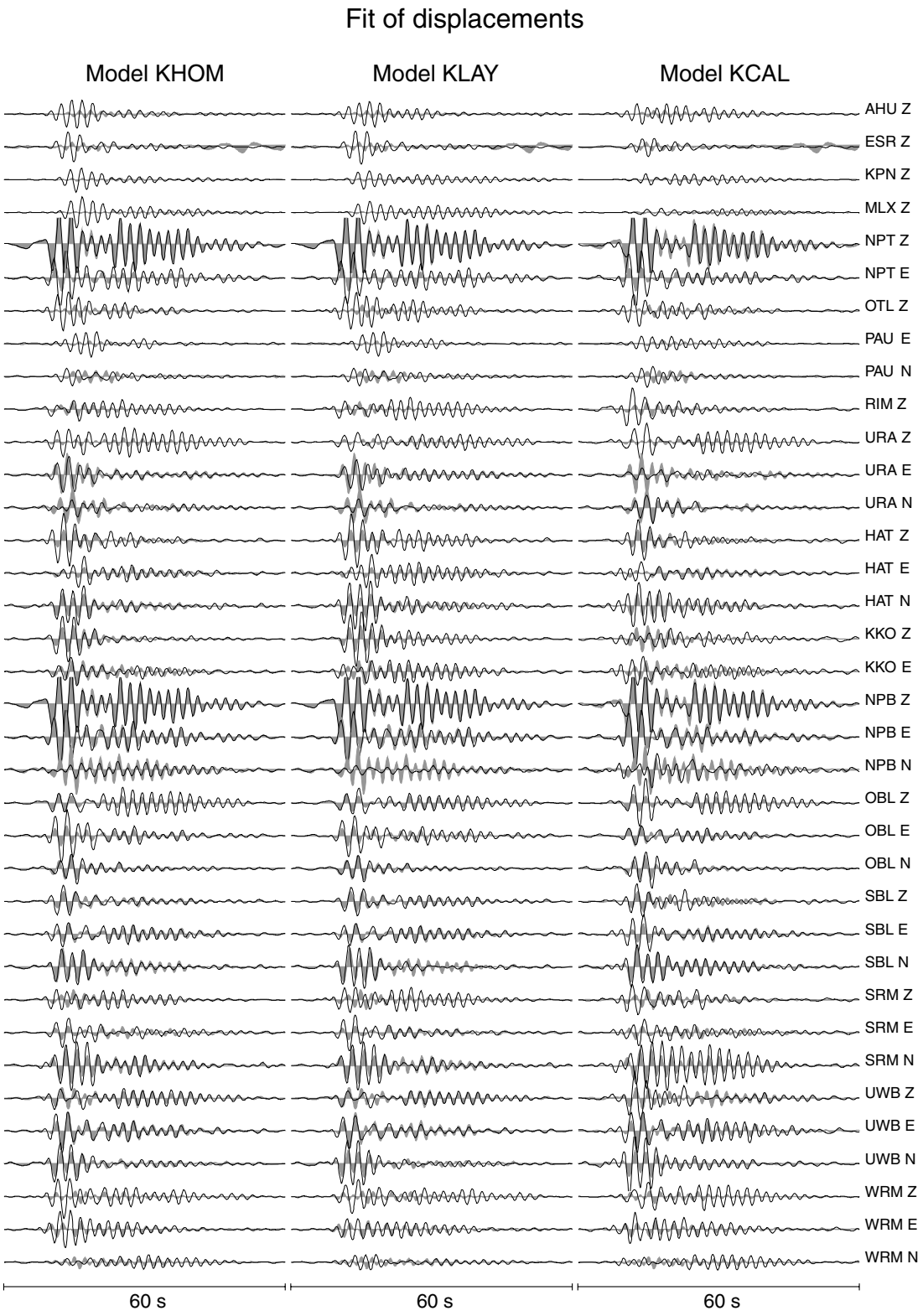

Figure 12. Fit of displacements for 3-D inversions assuming 3-D model KHOM (left-hand graph), KLAY (centre graph) and KCAL (right-hand graph). Displacements are plotted using grey shade, while thick black lines representing synthetic seismograms. All 36 traces used for the inversions are shown. Names of stations and components are given on the right of each set of traces.

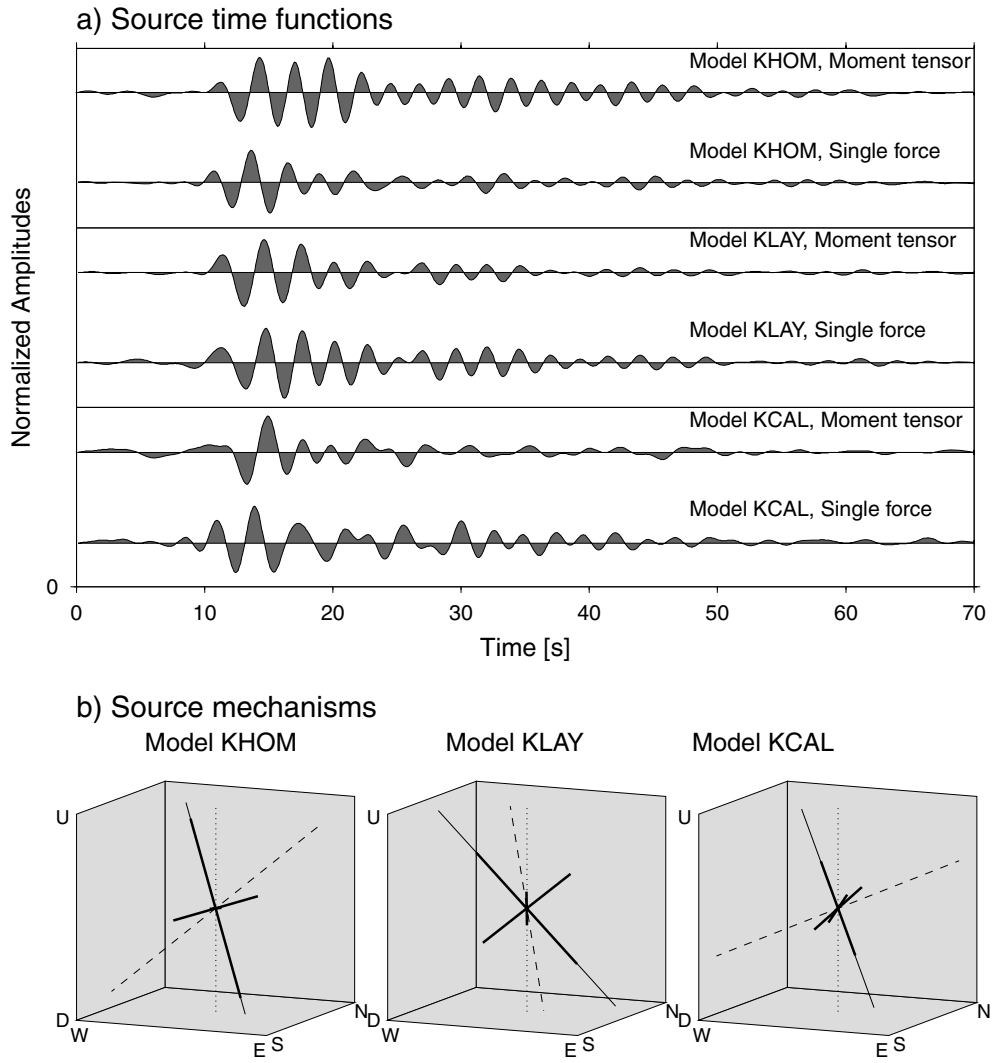

Figure 13. Results of 3-D inversions. (a) Normalized source time functions (STFs) retrieved when assuming different 3-D models. Moment tensor (MT) and single force (SF) components are shown, respectively, from top to bottom for models KHOM, KLAY and KCAL. (b) Orientation of eigenvectors (thick continuous lines), when assuming the same three velocity models. Amplitudes of eigenvectors are scaled to respective eigenvalues and crack axis (thin continuous line), force direction (dashed line) and vertical direction (dotted line) are also shown.

which indicated that a long lasting ringing source is required if assuming a homogeneous model. For this model, the complexity of the waveforms to fit is only achieved under the assumption of a complex time-behaviour of the source. On the contrary, the assumptions of layered (KLAY) or partially layered (KCAL) models, lead to the retrieval of a simpler STF.

The retrieved source geometry fits well with cracks of variable orientations. For all considered models, we obtain large diagonal moment tensor components, plus a minor double couple component (compressive toward East-Down), whereas remaining components are negligible. On the other hand, the resolution of all moment tensor components using the frequency domain inversion technique has been checked by a set of additional synthetic tests, which use different source mechanisms at shallow depths. For KHOM model, amplitudes of North, East and vertical components scale as (1:1:2). The relative amplitude of the East-West dipole component gets progressively larger for models KCAL and KLAY. These results are reflected in the consequent crack orientation. For model KHOM the eigenvectors defining the crack orientation are still scaling about (1:1:2); the solution points to a subhorizontal crack, with a minor dip angle, of about 18°, toward WNW direction. The orientation of the single force is dipping 44° toward WSW (azimuth 258°). The retrieved force component is aligned with fractures observed at the surface, pointing from the epicentral area toward ENE, but is not coplanar to the crack orientation retrieved from moment tensor components (with an angle of 37° between force direction and crack plane). A significant offset is retrieved between SF and MT source time functions, with SF component excitation preceding MT components excitation by 0.6 s. This observation may be interpreted in terms of a slug (SF) followed by oscillations of the crack wall (MT), which then interacts with the fluid. Owing to the problem complexity and the simplifications we assume in our model, this interpretation is, however, weakly constrained.

Best results are retrieved for model KCAL, for which we obtain a more dipping crack, with a dip angle 31° towards SW; eigenvectors scale again as (1:1:2). Results for KCAL model are significant with respect to the retrieved single force: with a dip angle of 16° and a strike of 247°, the single force is both coplanar with crack orientation

(the angle between force direction and crack plane is lower than 1°) and fits to the surface fissures orientation. Finally, for the case of the layered model (KLAY), moment tensor configuration cannot be strictly represented as a crack because two dipoles (east–west and up–down) have almost the same magnitude. The tensor cannot be rotated to a reference system, for which a dipole would dominate over the two remaining dipoles. The plot of eigenvectors (Fig. 13b) would point to an elongated crack, dipping in the same direction as for model KCAL, but with a larger dip angle of about 60°. The single force, which is almost vertical, is not consistent with the crack orientation. These anomalous results for model KLAY, in agreement with the worse retrieval of seismogram provided by the model, are interpreted as due to its unrealistically extended layering. Finally, in reference to the three proposed solutions, we have additionally assessed that single force components were necessary to improve the description of source behaviour, by applying the Akaike Information Criteria as discussed in the previous section. Results support the choice of a source model composed of both moment tensor and single forces.

While model KLAY leads to inconsistent results, models KHOM and KCAL both allow a better fit of the observed LP data. The assumption of a homogeneous medium, outside the caldera and far from the source region, is supported by our results. The retrieved mechanism and its time behaviour are indeed different depending on the description of heterogeneities inside the caldera. Both models point to a similar crack structure, with some differences with respect to the dipping of the crack plane. Major differences are related to the source time function. Under the assumption of a homogeneous source region, we obtain a ringing source, with a slow amplitude decay during almost 40 s. When the source region is described with more detail, in this case by means of a layered structure based on tomographic studies (Saccorotti *et al.* 2003), the resulting source behaviour is much simpler, in the sense that the source excitation significantly decays after 5–10 s. Both models KHOM and KCAL predict the presence of additional significant single forces, whose orientation is in agreement with the striking of the surface fissures which start at the Northwestern border of Halemaumau crater and extend towards WNW. The agreement between crack plane, single force and surface fissure orientation is better achieved for the more detailed model KCAL. Assuming this model, the shallow depth of the source would likely point to the interpretation of results in terms of the resonance of a subhorizontal hydrothermal crack. The short (about 10 s) resonance of the crack, which is derived from moment tensor STF, would be a consequence of fluid transfer along the crack plane and toward WNW, as suggested by the retrieval of the single force component. A second inversion for this model, using the alternative fitting procedure described in the end of Section 3 and based on a distance dependent data weighting, leaded to poorer results, with larger uncertainties. While the geometry of the crack is still consistently resolved, the time required for the release of the majority of the seismic energy slightly increases (∼15 s). Major discrepancies appear for the single force components, which are not well resolved anymore, and are much more contaminated by noise.

The comparison of inverted sources under the assumption of 1-D and 3-D models highlights the effects of topography and the improvements in the source retrieval, achieved by computing GFs with more detailed 3-D models. The larger misfits calculated for inversions including topography are related to the increased number of traces to be fitted: assuming a homogeneous model and using only those stations selected for the 1-D inversion (paragraph 5.1), the calculated misfit is 0.338 for the 3-D model versus 0.466 for the 1-D model. The introduction of topography in the modelling also improves the distinction between the radiation patterns associated with the different source components, helping to solve the ambiguity observed between M_{zz} and F_z radiation patterns in a flat geometry.

6 CONCLUSIONS

With this study, we identified important contributions of topographic features and heterogeneous velocity structures to the generation of LP waveform signatures. These contributions are extremely important to take into account for a correct inversion of seismic signals and the consequent interpretation of physical phenomena generating LP signals. Our results, arising from a wide set of synthetic tests, provide new insights for a better understanding of the source mechanisms associated with LP events. They suggest that long ringing monochromatic signals, such as the LP signal observed at Kilauea in May 2001, may be of a consequence of both source and path effects. To improve source inversions of LP events, the modelling of complex 3-D structures should be taken into account. Further improvement in the definition of velocity models and detailed tomographic studies will certainly add important information towards the better interpretation of LP data in volcanic regions.

Effects of crustal heterogeneities were analysed by a set of synthetic tests. The choice of simplified homogeneous models provides synthetic seismograms characterized by low amplitude surface waves. On the other hand, the introduction of realistic layering leads to the generation of ringing waveforms, where energy is radiated at surface receivers during a longer time. In particular, the combination of a shallow source and the presence of low velocity shallow structures plays a major role in the generation of significant surface waves: shallower sources, embedded in layers with increasingly lower velocities, produce surface waves with larger amplitudes. These results are in good agreement with those arising from the forward modelling carried out by Goldstein & Chouet (1994), who emphasized the importance of introducing a layered structure for a consistent determination of synthetic seismograms in the analysis of volcanic tremor and LP events. The presence of lateral discontinuities in the layering, tested for 2-D models representing simplified caldera structures, introduces significant modification of wave dispersion. Assuming the model named KCAL, which reproduces a velocity contrast at the caldera border, a reduced waveform dispersion is observed in the outer homogeneous region. A minor effect of the introduction of caldera-shaped lateral discontinuities, which is observed by comparing synthetic seismograms for fully layered (KLAY) and locally layered (KCAL) models, is the presence of delayed arrivals, driven by the interference of waveforms reflected at the lateral interfaces. As a consequence of the mentioned effects of the velocity structure on GFs signatures, the inversion of LP signals leads to different results, depending on the assumed crustal model. These effects can be seen even in a simplified approach using flat models to remove effects of topography. Inversion results for flat models show a significant variation of the retrieved STFs: the fit of LP data requires the retrieval of complex extended sources for homogeneous models, while short duration STFs are sufficient in the case of realistically layered models.

While the presence of layered structures is easily implemented by using reflectivity codes to generate GFs, the analysis of the effects of topography requires the use of numerical methods to calculate GFs for 3-D models which is done here based on a pseudo-spectral approach. The role of topography in the inversion of LP sources was studied by comparing inversion results for simplified flat models and 3-D models. Even with the difficulty to extrapolate a general

behaviour of synthetic seismograms depending on topographic features, some considerations can still be done. First, some differences were observed in terms of the source geometry retrieved from the inversion using different models, indicating effects of topography on synthetic GFs. A second important effect is related to the artificial retrieval of single force components with the unrealistic assumption of flat models: this problem arises from the difficulty, given the flat model geometry, to distinguish between radiation patterns associated with certain moment tensor components and single force components. A clear improvement for the retrieval of significant single forces was achieved by using 3-D models with topography. Although the use of flat models can be helpful to check the effects of other model parameters and to better constrain the source depth, as shown for the studied LP event. Results generally indicate that the introduction of topography clearly leads to an improvement of the inversion results. Effects of topography are likely to be even more significant in steeper volcanic areas.

Finally, the application of 3-D models with different velocity structures allowed the retrieval of the source mechanism for an LP event, observed at Kilauea caldera in 2001 May. Models KCAL and KHOM consistently point to a source with a subhorizontal crack geometry plus a single force. The fully layered model leads to poorer results, suggesting that the assumed layered velocity structure is incorrect outside the caldera. The results arising from model KCAL, which assumes a very shallow source, are interpreted in terms of a fluid transfer (single force) and the consequent resonance of the crack, whose amplitude decays significantly in the first 10 s. Single force is coplanar with the crack plane (which is dipping 31° towards SW) and oriented ENE–WSW (strike 67°) consistently with fissures observed on the caldera surface. Owing to the shallow location, the source of the LP event is interpreted as associated with the hydrothermal system, as also suggested by Almendros *et al.* (2001b). The mentioned surface fissures would, therefore, be associated with the same system, and likely present gas release during the activity period. Although permanent degassing has been observed at those fissures, there is no measurement or observation, which could attest of a burst in degassing at the moment of the LP event.

ACKNOWLEDGMENTS

This work has been partially funded by the SPICE project (Contract Number MRTN-CT2003-504267) of the European Commission's Human Resources and Mobility Programme.

REFERENCES

Akaike, H., 1974. A new look at the statistical model identification, *IEEE Trans. Autom. Contr.,* **AC-9,** 716–723.

Aki, K. & Richards, P. G., 1980. *Quantitative Seismology,* W.H. Freeman, New York, pp. 932.

Almendros, J., Chouet, B. & Dawson, P., 2001a. Spatial extent of a hydrothermal system at Kilauea volcano, Hawaii, determined from array analysis of shallow long-period seismicity. Part I: method, *J. geophys. Res.,* **106,** 13 565–13 580.

Almendros, J., Chouet, B. & Dawson, P., 2001b. Spatial extent of a hydrothermal system at Kilauea volcano, Hawaii, determined from array analysis of shallow long-period seismicity. Part II: results, *J. geophys. Res.,* **106,** 13 581–13 597.

Almendros, J., Chouet, B., Dawson, P. & Huber, C., 2002. Mapping the sources of the seismic wave field at Kilauea volcano, Hawaii, using data recorded on multiple seismic antennas, *Bull. seism. Soc. Am.,* **92,** 2333–2351.

Ashford, S., Sitar, N., Lysmer, J. & Deng, N., 1997. Topographic effects on the seismic response of steep slopes, *Bull. seism. Soc. Am.,* **87,** 701–709.

Auger, E., D'Auria, L., Martini, M., Chouet, B. & Dawson, P., 2006. Real-time monitoring and massive inversion of source parameters of very long period seismic signals: an application to Stròmboli Volcano, Italy, *Geophys. Res. Lett.,* **33,** doi:10.1029/2005GL024703.

Battaglia, J. & Aki, K., 2003. Location of seismic events and eruptive fissures on the Piton de la Fournaise volcano using seismic amplitudes, *J. geophys. Res.,* **108**(B8), doi:10.1029/2002JB002193.

Battaglia, J., Got, J.-L. & Okubo, P. G., 2003. Location of Long-Period events below Kilauea using seismic amplitudes and accurate relative relocation, *J. geophys. Res.,* **108**(B12), 2553, doi:10.1029/2003JB002517.

Bouchon, M., Schultz, C. A. & Toksöz, M. N., 1996. Effect of three-dimensional topography on seismic motion, *J. geophys. Res.,* **101,** 5835–5846.

Cesca, S. & Dahm, T., 2007. A frequency domain inversion code to retrieve time-dependent parameters of very long-period volcanic sources. *Comput. Geosci.,* **34,** 235–246.

Cesca, S., Braun, T., Tessmer, E. & Dahm, T., 2007. Modelling of the April 5, 2003 Stròmboli (Italy) paroxysmal eruption from the inversion of broadband seismic data, *Earth plant. Sci. Lett.,* **261,** 164–178.

Cervelli, P. & Miklius, A., 2003. The shallow magmatic system of Kilauea volcano, UG Geol. Surv. Prof. Pap., The Puu Oo-Kupaianaha Eruption of Kilauea Volcano, *Hawaii: The First 20 Years,* **1676,** 149–164.

Chouet, B. A., 1996. Long-period volcano seismicity: its source and use in eruption forecasting, *Nature,* **380,** 309–316.

Chouet, B. *et al.*, 2003. Source mechanisms of explosions at Stromboli Volcano, Italy, determined from moment-tensor inversions of very-long-period data, *J. geophys. Res.,* **108,** 1–25, doi:10.1029/2002JB001919.

Dawson, P. B., Chouet, B. A., Okubo, P. G., Villaseñor, A. & Benz, H. B., 1999. Three-dimensional velocity structure of the Kilauea caldera, Hawaii, *Geophys. Res. Lett.,* **26,** 2805–2808.

Geli, L., Bard, P. Y. & Jullien, B., 1988. The effect of topography on earthquake ground motion: a review and new results, *Bull. seism. Soc. Am.,* **78,** 42–63.

Goldstein, P. & Chouet, B., 1994. Array measurements and modeling of sources of shallow volcanic tremor at Kilauea Volcano, Hawaii, *J. geophys. Res.,* **99,** 2637–2652.

Heimann, S., 2005. Numerische Modellierung der Nachgiebigkeit des Meeresbodens mit einer Tschebyscheff-Fourier-Methode, *Degree thesis*, University of Hamburg, Hamburg, Germany, pp. 50.

Hill, N. R. & Levander, A. R., 1984. Resonance of low velocity layers with lateral variations, *Bull. seism. Soc. Am.,* **74,** 521–537.

Ingebritsen, S. E. & Scholl, M. A., 1993. The hisrology of Kilauea volcano, *Geothermics,* **22,** 255–270.

Kumagai, H., Chouet, B. A. & Dawson, P. B., 2005. Source process of a long-period event at Kilauea Volcano, Hawaii, *Geophys. J. Int.,* **161,** 243–254.

Monteiller, J. Got, J.-L., Virieux, J. & Okubo, P., 2005. An efficient algorithm for double-difference tomography and location in heterogeneous media, with an application to Kilauea volcano, *J. geophys. Res.,* **110,** doi:10.1029/2004JB003466.

Müller, 1985. The reflectivity method: a tutorial, *J. Geophys.,* **58,** 153–174.

Neuberg, J. & Pointer, T., 2000. Effects of volcano topography on seismic broad-band waveforms, *Geophys. J. Int.,* **143,** 239–248.

Nguyen, X. N., Dahm, T. & Grevemeyer, I., 2007. Inversion of Scholte wave dispersion and waveform modelling for the Ninetyeast Ridge region, *J. Seismol.,* submitted.

Ohminato, T. & Chouet, B. A., 1997. A free-surface boundary condition for including 3D topography in the finite-difference method, *Bull. seism. Soc. Am.,* **87,** 494–515.

Ohminato, T., Chouet, B. A., Dawson, P. & Kedar, S., 1998. Waveform inversion of very long period impulsive signals associated with magmatic injection beneath Kilauea Volcano, Hawaii, *J. geophys. Res.,* **103,** 23 839–23 862.

Olsen, K. B., Pechman, J. C. & Schuster, G. T., 1995. Simulation of 3-D elastic wave propagation in the Salt Lake Basin, *Bull. seism. Soc. Am.,* **85,** 1688–1710.

Ripperger, J., Igel, H. & Wassermann, J., 2003. Seismic wave simulation in the presence of real volcano topography, *J. Volcanol. Geotherm. Res.,* **128,** 31–44.

Saccorotti, G., Chouet, B. & Dawson, P., 2001. Wavefield properties of a shallow long-period event and tremor at Kilauea volcano, Hawaii, *J. Volcanol. Geotherm. Res.,* **109,** 163–189.

Saccorotti, G., Chouet, B. & Dawson, P., 2003. Shallow-velocity models at the Kilauea Volcano, Hawaii, determined from array analyses of tremor wave fields, *Geophys. J. Int.,* **152,** 633–648.

Tessmer, E., Kosloff, D. & Behle, A., 1992. Elastic wave propagation simulation in the presence of surface topography, *Geophys. J. Int.,* **108,** 621–632.

Vasco, D. W., 1989. Deriving source-time functions using principal component analysis, *Bull. seism. Soc. Am.,* **79,** 711–730.

Wen, S., Chang, W. Y. & Chen, C. H., 2007. Seismic wave propagation in basin structures from numerical modelling, *Terr. Atmos. Ocean Sci.,* **18,** 1–7.